ACCEPTED MANUSCRIPT:

John McCloy, Jose Marcial, Deepak Patil, Muad Saleh, Mostafa Ahmadzadeh, Hua Chen, Jarrod Crum, Brian Riley, Hrishikesh Kamat, Antoine Brehault, Ashutosh Goel, Kristian Barnsley, John V. Hanna, Prashant Rajbhadari, Claire Corkhill, Russell Hand, Neil Hyatt, "Glass structure and crystallization in boro-alumino-silicate glasses containing rare earth and transition metal cations," *MRS Advances*, 4(17-18), 1029-1043 (2019).
https://doi.org/10.1557/adv.2019.99

Glass structure and crystallization in boro-alumino-silicate glasses containing rare earth and transition metal cations: a US-UK collaborative program

John S. McCloy,[1,2] José Marcial,[1] Deepak Patil,[1] Muad Saleh,[1] Mostafa Ahmadzadeh,[1] Hua Chen,[1,6]

Jarrod V. Crum,[2] Brian J. Riley,[1,2]

Hrishikesh Kamat,[3] Antoine Bréhault,[3] Ashutosh Goel,[3]

Kristian E. Barnsley,[4] John V. Hanna[4]

Prashant Rajbhandari,[5] Claire L. Corkhill,[5] Russell J. Hand,[5] Neil C. Hyatt[5]

[1]*Washington State University, Pullman, WA, USA*

[2]*Pacific Northwest National Laboratory, Richland, WA, USA*

[3]*Rutgers University, New Jersey, USA*

[4]*University of Warwick, Coventry, UK*

[5]*University of Sheffield, Sheffield, UK*

[6]*Inner Mongolia University of Science and Technology, China*

ABSTRACT

Nuclear wastes generated from reprocessing of used nuclear fuel tend to contain a large fraction of rare earth (RE, e.g., Nd^{3+}), transition (TM, e.g., Mo^{6+}, Zr^{4+}), alkali (A, e.g., Cs^{+}), and alkaline earth cations (AE, e.g., Ba^{2+}, Sr^{2+}). Various strategies have been considered for immobilizing such waste streams, varying from nominally crystal-free glass to glass-ceramic to multi-phase ceramic waste forms. For glass and glass-ceramic waste forms, the added glass-forming system is generally alkali-alkaline earth-aluminoborosilicate (i.e., Na-Ca-Al-B-Si oxide). In a US-UK collaborative project, summarized here, we investigated the glass structure and crystallization dependence on compositional changes in simulated nuclear waste glasses and glass-ceramics. Compositions ranged in complexity from five – to – eight oxides. Specifically, the roles of Mo and rare earths are investigated, since a proposed glass-ceramic waste form contains crystalline phases such as powellite [(AE,A,RE)MoO_4] and oxyapatite [(RE,AE,A)$_{10}Si_6O_{26}$], and the precipitation of molybdenum phases is known to be affected by the rare earth concentration in the glass. Additionally, the effects of other chemical additions have been systematically investigated, including Zr, Ru, P, and Ti. A series of studies were also undertaken to ascertain the effect of the RE size on glass structure and on partitioning to crystal phases, investigating similarities and differences in glasses containing single RE oxides of Sc, Y, La, Ce, Nd, Sm, Er, Yb, or Lu. Finally, the effect of charge compensation was investigated by considering not only the commonly assessed peralkaline glass but also metaluminous and peraluminous compositions. Glass structure and crystallization studies were conducted by spectroscopic methods (i.e., Raman, X-ray absorption, nuclear magnetic resonance (NMR), optical absorption, photoluminescence, photoluminescence excitation, X-ray photoelectron spectroscopy), microscopy (i.e., scanning electron microscopy, transmission electron microscopy, electron probe microanalysis), scattering (i.e., X-ray and neutron diffraction, small angle measurements), and physical characterization (i.e., differential thermal analysis, liquidus, viscosity, density). This paper will give an overview of the research program and some example unpublished results on glass-ceramic crystallization kinetics, microstructure, and Raman spectra, as well as some examples of the effects of rare earths on the absorption, luminescence, and NMR spectra of starting glasses. The formal collaboration described here has resulted in the generation of a large number of results, some of which are still in the process of being published as separate studies.

1. BACKGROUND

Introduction

An innovative glass-ceramic waste form is being developed by the US Department of Energy (DOE) to immobilize non-fissionable waste streams of alkali(A)/alkaline-earths(AE) (e.g., ^{137}Cs, ^{90}Sr), rare earth (RE), and transition metals (TM) generated by the projected TRUEX^{plus} process [1]. The target crystalline phase assemblage comprises powellite, oxyapatite, and lanthanide borosilicate phases.

Fundamental mechanistic understanding of thermodynamic phase transitions and crystallization mechanisms occurring during synthesis of this glass-ceramic (as a function of thermal history and glass chemistry) is of paramount importance for international waste management programs, which seek to exploit glass-ceramic technology or, conversely, optimize conventional borosilicate glasses to improve the solubility of key fission products [2, 3]. This approach is also critically important in the UK scenarios, where glass-ceramics offer key advantages for post-operative clean out of Mo-rich residues from high-level waste storage tanks [4], disposition of plutonium residues, and efficient waste immobilization for advanced fuel cycles, to meet the aims of the UK Nuclear Industry Strategy [5, 6].

This paper presents an overview of the work accomplished in the framework of an US – UK collaborative research project aimed at understanding the **(1)** fundamental mechanisms of the *phase transitions* leading to the conversion of melt to a multiphase glass-ceramic as a function of composition and cooling rate; and **(2)** influence of *glass chemistry* on kinetics of phase separation and crystallization. These objectives were realized through the performance of three inter-related tasks including **(i)** understanding kinetics of phase separation and crystallization in baseline glasses [7], **(ii)** influence of glass chemistry [8, 9] on phase transitions and chemical durability, and **(iii)** *in-situ* high-temperature studies [10]. The project aimed to advance our understanding about the fundamental science on the kinetics and mechanisms of liquid-liquid phase separation and crystallization of complex multi-phase glass-ceramics for immobilization of mixed alkali/alkaline earth, rare earth, and transition metal waste streams.

Waste form description

A key barrier to maturation and exploitation of glass-ceramic technology is the gap in our fundamental understanding of the molecular-scale mechanisms of phase separation and crystallization that lead to the development of the desired phase assemblage and microstructure that can determine long-term product performance. Since the projected waste stream is expected to be rich in MoO_3 (~14 mass%), alkaline earths (e.g., SrO, BaO ~ 11 mass%), and alkalis (e.g., Rb_2O, Cs_2O ~12 mass%), the presence of these species in the waste feed will result in a tendency towards liquid-liquid phase separation and (uncontrolled) crystallization of ternary molybdates [11, 12] due to the high ionic field strength of the Mo^{VI} cation (1.89–1.94 $Å^{-2}$). Therefore, the challenge is in *predictably* achieving the targeted phase assemblage and microstructure, requiring a detailed understanding of the transformation process as a function of both cooling rate and melt chemistry. Controlling this phase separation and the crystallization process is critical to prevent the formation of a non-durable crystal, glass, or crystal-glass interface. For example, it is known that uncontrolled crystallization of $(RE, A, AE)_{10}Si_6O_{26}$ oxyapatite results in alkali enrichment of the interfacial glass region, leading to deleterious and unpredictable leaching behavior [13, 14].

The proposed glass-ceramic waste form in question is expected to double the waste loading (to ~45 mass%) and exhibit improved thermal stability in comparison to the baseline alkali borosilicate glass waste form. The abovementioned benefits are achieved by partitioning the insoluble fission products into a suite of ceramic phases, through controlled crystallization. Powellite (i.e., $AEMoO_4$), oxyapatite [i.e., $(RE,AE,A)_{10}Si_6O_{26}$], rare earth borosilicate (i.e., $RE_3BSi_2O_{10}$), and pollucite (i.e., $AAlSi_2O_6$) comprise the target phase assemblage. Preliminary research on these compositions with crucible melt studies [1] and a pilot-scale cold-crucible induction melter (CCIM) [2] demonstrated melting temperatures of ~1350°C, allowing melting of atypical refractory compositions. The transformation process upon slow cooling begins with liquid-liquid phase separation of Mo-rich and RE-rich droplets in a borosilicate matrix, followed by crystallization. Differences in melt chemistry and cooling history, due to the variable distance from the canister centerline, control the final microstructure.

Per the current DOE plan [3], the assumed process for allowing the crystalline phases to form in canisters is through controlled cooling from melts (without reheating). In such a scenario, it becomes crucial to understand the phase transitions, and respective temperatures, leading to the conversion of a melt to a multiphase glass-ceramic waste form as a function of cooling rate. Additionally, a significant amount of data has been collected on phase separation and crystallization in the *slow-cooled* (SC) glass-ceramics [1, 2]. However, due to the compositional complexity of these glasses, as well as issues associated with volatility during *in-situ* thermal analysis, it has been difficult to accurately determine the temperatures at which liquid-liquid phase separation and crystallization occur.

2. COMPOSITIONAL STUDIES

The glass-ceramic waste forms are compositionally complex, and previous fundamental studies focused on glasses that are too simplified to address all the important compositional variables. Therefore, an 8-oxide simplified composition was proposed (i.e., SiO_2–Nd_2O_3–CaO–Na_2O–B_2O_3–Al_2O_3–MoO_3–ZrO_2), which was then modified to study the individual and combined effects of other elements. The strategy has been to carefully formulate glasses complex enough to be relevant to the proposed waste forms, but simple enough to allow assessment of compositional effects. Using a combination of studies of different designs, the relative effects of Na_2O/CaO, Na_2O/B_2O_3, Na_2O/Al_2O_3, Na_2O/ZrO_2, and MoO_3/Nd_2O_3 were investigated. Table 1 presents the compositions of multicomponent glass systems studied in the framework of this project (note that the nomenclature adopted for the glass series in this table may not precisely match that of the cited publications, but is intended to present the compositional space in a uniform way to compare across studies). These studies were designed with an aim to capture the essential components of the proposed US glass-ceramic waste form in appropriate proportions and ranges, address specific UK compositional needs, and allow definitive understanding of chemical effects. One metric used to compare glasses is the concentration of excess Na_2O, defined as $Na_2O\_excess = Na_2O-Al_2O_3-ZrO_2$ (by mole) [15]. When this quantity is >0, the glass is *peralkaline*, meaning that enough Na_2O is available to charge compensate all AlO_4^- species and all ZrO_6^{2-} species [16]. If this quantity is <0, the glass is *peraluminous*, meaning that there is inadequate Na_2O available to keep Al and Zr dissolved in the glass, and some other modifier (such as Ca or RE) must take this role. When $Na_2O\_excess = 0$, this is known as the *metaluminous* composition. In this calculation, no assumptions have been made about the boron speciation or the need for BO_4^- MoO_4^- or RE species charge compensation.

In general, these glass and heat-treated glass-ceramic systems were characterized by some or all of the following techniques: visual investigation, scanning electron microscopy (SEM), SEM with energy dispersive spectroscopy (EDS), electron probe microanalysis (EPMA) using wavelength dispersive spectroscopy (WDS), X-ray diffraction (XRD), magic angle spinning – nuclear magnetic resonance (MAS NMR), X-ray absorption (XAS) [including X-ray absorption near edge spectroscopy (XANES) and extended X-ray absorption fine structure (EXAFS)], X-ray photoelectron spectroscopy (XPS), differential thermal analysis (DTA), Raman spectroscopy, optical absorption, and combined excitation-emission spectroscopy (CEES) [including photoluminescence (PL) and photoluminescence excitation (PLE)].

Table 1. Glass compositions (in mol%) produced in this US/UK joint program. Where *x* is listed in the glass series name, it is placed before the primary compositional variable for that study.

Glass series	SiO_2	B_2O_3	Al_2O_3	MoO_3	ZrO_2	Na_2O	CaO	RE_2O_3 (RE_2O_3 _tot)†	Others	Na_2O _exc	Type#	Ref
Na-*x*Mo	60-*x*	10	5	*x*=0-4	3.5	25	-	-	-	20.0	Peralk	[8]
Ca-*x*Mo	60-*x*	10	5	*x*=0-4	3.5	12.5	12.5	-	-	7.5	Peralk	[8]
Re-*x*Mo	55-*x*	10	5	*x*=0-4	3.5	12.5	12.5	5	-	7.5	Peralk	[8]
SS-Nd-*x*Mo	49.7	11.0	3.0	*x*=0-6.8*	3.1	12.3	16.4	4.5	-	-	Peralk	-
SS-La-*x*Mo	51.2	11.3	3.1	*x*=0-6.8*	3.2	12.7	16.8	4.6	-	-	Peralk	-
SS-Mo-*x*La	51.2	11.3	3.1	1.6	3.2	12.7	16.8	*x*=1.6-4.6*	-	-	Peralk	-
SS-*x*La; SS-*x*Lu	52.0	11.5	3.1	-	3.3	12.9	17.1	*x*=0-4.7*	-	-	Peralk	-
x(La+Ce)	50	11.8	5.1	3.5	3.1	12.0	13.5	*x*=(1.0-4.9)*	-	3.8	Peralk	-
*RE*NaCaMo	48.0	11.4	4.9	3.4	3.0	11.5	12.9	4.9	-	3.7	Peralk	[9]
La-Nd; La-Er	48.0	11.4	4.9	3.4	3.0	11.5	12.9	(4.9)	-	3.7	Peralk	-
LaNaCa	49.7	11.8	5.1	-	3.1	11.9	13.4	5.1	-	3.8	Peralk	[9]
NaCaMo	50.5	12.0	5.1	3.5	3.2	13.6	12.1	-	-	3.9	Peralk	[9]
LaCaMo	48.0	11.4	4.9	3.4	3.0	-	24.5	4.9	-	-7.9	Peralum	[9]
LaMo	63.6	15.0	6.5	4.5	4.0	-	-	6.5	-	-10.4	Peralum	[9]
SS-RE-4.6	48.8	10.8	2.9	1.6	3.0	12.1	16.1	4.6	-	-	Peralk	-
10B-10RE	50	10	5	4	3	9	9	10	-	1.0	Metalum	-
15B-10RE	50	15	5	4	3	6.5	6.5	10	-	-1.5	Peralum	-
SS-MoNd-*x*Ti	47.1	10.4	2.8	5	2.9	11.7	15.5	4.3	1-4 TiO_2*	-	Peralk	-
REMo-*x*Zr	52-*x*	10	5	3	*x*=1-4	12.5	12.5	5	-	-	Peralk	-
REMoZr-*x*Ru	50-*x*	10	5	3	4	12.5	12.5	5	*x*=0.05-0.4 RuO_2	-	Peralk	-

*with increased concentration of this component, the rest of the glass composition is normalized, keeping proportions constant. The stoichiometry shown is for the lowest fraction of this indicated component. The number after the dash ('-') indicates the highest fraction tested;
†tot_RE_2O_3 is total of all rare earth oxides, calculated as trivalent cations.
#Peralk = peralkaline; Peralum = peraluminous; Metalum = metaluminous

Effect of Mo concentration

The first completed fundamental study involved investigating the solubility of molybdenum in increasingly complex aluminoborosilicate glasses containing zirconia (i.e., 5–8 oxide components); this was accomplished first with only Na_2O, then substituting half of the Na_2O for CaO, and finally adding 5 mol% Nd_2O_3 to the former [8]. All glasses were peralkaline. Glasses and glass-ceramics were investigated with XRD, NMR (i.e., ^{11}B, ^{27}Al, and ^{29}Si), SEM-EDS, EPMA, XPS (i.e., Mo and Nd), liquidus temperature, and chemical analysis (inductively coupled plasma-optical emission spectroscopy, or ICP-

OES, for target versus measured Mo dissolved in glass). This study resulted in the proposition of a novel three-step mechanism to explain the higher solubility of MoO_3 in alkali/alkaline-earth aluminoborosilicate glasses as a function of Nd_2O_3 content as follows. In Step 1, a fraction of RE cations distribute themselves in the borate-rich areas of glass while the remaining RE cations cluster in the silicate/borosilicate region. In Step 2, the MoO_4^{2-} ions are incorporated into the RE borate phase, thus forming a stable RE-Mo-B-O glassy region. In Step 3, any further increase in MoO_3 concentration is likely to exceed the concentration of molybdate ions that could be accommodated in the Nd_2O_3–MoO_3–B_2O_3 glassy structure, thus leading to crystallization of Nd-rich $CaMoO_4$.

A follow-up to this study involved investigating the isothermal and non-isothermal and crystallization kinetics of the molybdenum- and RE-containing glasses. The non-isothermal DTA scans were collected for the studied glasses at four different heating rates to calculate the activation energies of crystallization, while isothermal heat treatments were made at temperatures in the range of 700 to 1200°C at an increment of 100°C with a dwell time of 1 h at the target temperature. Heat-treated glasses were investigated by XRD and Raman spectroscopy to assess the crystalline phase evolution. These results have been discussed in the current paper.

Additionally, an 8-oxide "simplified Sellafield" composition was investigated as a function of molybdenum concentration. A baseline composition was made without MoO_3, and subsequent glasses increased this component while keeping the proportions of the other constituents constant. This series has been denoted as "SS-Nd-*x*Mo," where *x* indicates that MoO_3 concentration is varied, here from 0 to 12 mass% (0–6.8 mol%). Glasses were melted and crystallized, and studied by XRD, Raman spectroscopy, thermal analysis, and SEM. Detailed results of this study will be published elsewhere.

Effect of rare earth concentration

Several 7- or 8-oxide "simplified Sellafield" compositions were investigated to assess the effects of increasing RE oxide concentrations. Some series contained MoO_3, and some did not. A baseline composition with MoO_3 was fixed with zero RE oxide, and subsequent glasses increased Nd_2O_3 while keeping the proportions of the other constituents constant. This series is denoted "SS-Mo-*x*Nd," where *x* indicates the Nd_2O_3 concentration is varied, here from 0 to 20 mass% (0–4.8 mol%). Since Nd_2O_3 makes NMR analysis difficult due to its paramagnetism, a series of glasses were formulated with non-paramagnetic RE cations. One series of glasses used fixed MoO_3 concentration (1.6 mol%) and increased La_2O_3 ("SS-Mo-*x*La," varying La_2O_3 0–4.6 mol%. Another was formulated with no MoO_3 and with increasing La_2O_3 concentration ("SS-*x*La") or Lu_2O_3 concentration ("SS-*x*Lu"). The third series of glasses "SS-La-*x*Mo" was also prepared. This time the La_2O_3 concentration was fixed at 4.6 mol%, and MoO_3 concentration was varied 0–4.6 mol%. Only the glass series "SS-Mo-*x*La" and "SS-La-*x*Mo" were labeled with Mo-95 oxide for a NMR study. All the glasses were synthesized by standard melt-quenching technique method. In the first step, physicochemical properties of the glasses such as thermal behavior, density and chemical durability (product consistency test) were studied, followed by the study of the effect on structure due to increasing La_2O_3 or MoO_3 by implementing XRD, SEM, Raman spectroscopy, and NMR (^{11}B, ^{29}Si, ^{95}Mo). Detailed results of these studies will be published elsewhere.

To test the effect of two simultaneous RE oxides with different nominal valences, a series of glasses were formulated with equimolar fractions of La_2O_3 and Ce_2O_3 (note, formulated and calculated as Ce_2O_3 but batched as CeO_2). Compositions were as follows (in mol%): $12.14\ Na_2O - 13.58\ CaO - 3.15\ ZrO_2 - 3.53\ MoO_3 - 5.14\ Al_2O_3 - 11.95\ B_2O_3 - 50.51\ SiO_2)_{100-x} - (x/2)La_2O_3 - (x/2)Ce_2O_3$ where x = 0, 1, 2, 3, 4 and 4.93. Glasses and crystallized glasses were studied by XRD, Raman spectroscopy, SEM, EPMA, and optical absorption. Note that the x=0 glass is the same as "NaCaMo" glass (see Table 1). Results of this study will be published elsewhere.

Effect of rare earth identity

The second completed fundamental study looked at the effect on crystallization of a peralkaline 8-oxide glass where the RE composition was kept fixed, but the single RE oxide was varied [9]. Here the RE oxides included La_2O_3, Ce_2O_3, Nd_2O_3, Sm_2O_3, Er_2O_3, and Yb_2O_3. Additionally, single components were removed (i.e., MoO_3, RE_2O_3, Na_2O, or Na_2O+CaO) and the composition renormalized. Specific nomenclature for these various glasses are provided in Table 1. Glasses and glass-ceramics were investigated by XRD, Raman spectroscopy, SEM-EDS, EPMA, as well as XAS and EXAFS (for Mo). It was shown that RE ions were present in not only the oxyapatite phase but also the powellite phase. For the smallest RE tested here, Yb_2O_3, very little oxyapatite formed, and keiviite ($Yb_2Si_2O_7$) formed instead. As a follow-up to this study, several other RE oxides were tested to investigate the small paramagnetic cations (i.e., Lu_2O_3, Y_2O_3, and Sc_2O_3), which were compared with previously obtained data on La_2O_3. Additionally, optical absorption and CEES (PL/PLE maps) were obtained on selected samples. Some of these results are discussed in the current paper.

The simplified Sheffield composition was modified to test the relative effects of the RE oxides, including La_2O_3, Nd_2O_3, Gd_2O_3, Ho_2O_3, and Lu_2O_3. These glasses are denoted "SS-RE-4.6." In this series, the impact of various RE oxides, especially on chemical environment of Mo in the glass matrix, was investigated by XRD, Raman spectroscopy, XAS and EXAFS (for Mo). Detailed results will be published elsewhere.

Several glasses were also produced with two RE oxides together with the sum equaling the same amount as above (i.e., 4.9 mol% RE_2O_3). These studies used La_2O_3 as an end-member with Nd_2O_3 or Er_2O_3. This allowed optical absorption and NMR as a function of the added amount of optically active paramagnetic rare earth. The two series investigated were the La-Nd series, with nominal composition 11.54 Na_2O – 12.91 CaO – 2.99 ZrO_2 – 3.36 MoO_3 – (4.93 – x) La_2O_3 – x Nd_2O_3 – 4.89 Al_2O_3 – 11.36 B_2O_3 – 48.02 SiO_2 (mol%) (where x = 0, 0.93, 2.93, 4.93) and the La-Er series with nominal composition 11.54 Na_2O – 12.91 CaO – 2.99 ZrO_2 – 3.36 MoO_3 – (4.93 – x) La_2O_3 – x Er_2O_3 – 4.89 Al_2O_3 – 11.36 B_2O_3 – 48.02 SiO_2 (mol%) (where x = 0, 0.93, 1.93, 2.93, 3.93, 4.93). Details of this work will be published elsewhere.

Effect of sodium concentration

An important consideration in the crystallization behavior of these materials is the relative availability of charge compensators such as Na_2O and, in some cases, CaO or RE_2O_3. To a first approximation, this can be assessed as Na_2O_excess, as described previously. Several glasses were specifically formulated to investigate this effect, including LaCaMo (all Na_2O, by mole, replaced by CaO) and LaMo (all Na_2O and CaO removed, and the rest of the glass composition normalized). Both glasses were peraluminous. LaCaMo appeared homogeneous when quenched, but, when heat-treated, produced powellite crystals and amorphous phase-separated SiO_2 [9]. LaMo appeared somewhat phase separated on quenching, but this was difficult to quantify; when heat-treated, multiple large-scale glass-in-glass phase separation was observed, with one phase enriched in B-Mo-La and one enriched in Si, and only minor crystallization of zircon ($ZrSiO_4$) [9].

Two other glass series were formulated specifically to look at the effects of low Na_2O concentrations and to explore the formation of the lanthanide borosilicate crystalline phase (i.e., $RE_3BSi_2O_{10}$), which had been reported previously in only a few compositions

[1]. The glass compositions for investigation of this phase were determined by statistically investigating the compositional effects on the appearance of this phase. A database of 53 complex glass compositions with quantitative crystallization information from XRD was used as an input to a statistical partitioning model [17]. Considering only the components SiO_2, Al_2O_3, Na_2O, CaO, Nd_2O_3, and MoO_3, it was determined that oxyapatite formation was favored in glass compositions with relatively low B_2O_3 (<13 mass%), low SiO_2 (<52 mass%), high Nd_2O_3 (>3 mass%), and low CaO (<12 mass%). Instead, when all alkali, alkaline earth, and RE components were binned as A_2O, AEO, and RE_2O_3, respectively, the B_2O_3 and SiO_2 partitions remained, but the third became low A_2O (<7 mass%). Similarly, for $RE_3BSi_2O_{10}$, when SiO_2, Al_2O_3, Na_2O, CaO, Nd_2O_3, and MoO_3 were considered, high Nd_2O_3, high B_2O_3, and low Na_2O were predictors of this phase. When the binned alkali, alkaline earth, and rare earths were considered, high RE_2O_3 (>8 mass%) and high B_2O_3 (>12 mass%) were predictors of the $RE_3BSi_2O_{10}$ formation.

Based on these tendencies, two glasses were formulated with high fractions of RE_2O_3 (10 mol%). One was formulated with an equimolar amount of B_2O_3 (10 mol%) and the other with more B_2O_3 (15 mol%). The SiO_2 content was kept constant at 50 mol%, Al_2O_3 at 5 mol%, MoO_3 at 4 mol%, and ZrO_2 at 3 mol%. The balance of the glass composition was split by mole for Na_2O and CaO, resulting in 1) a B/RE = 1, near metaluminous glass, with Na_2O = CaO = 9 mol%; and 2) a B/RE = 1.5, peraluminous glass, with Na_2O = CaO = 6.5 mol% (see Table 1). These glasses were tested as a function of RE identity, with more variations being made on the so-called 15B-10RE series, as it demonstrated more varied and interesting crystallization tendencies, which depended on RE size. XRD, SEM, and EPMA have been collected on these glasses, and the results will be presented elsewhere.

Several additional glasses were made with very simplified compositions in the peralkaline, metaluminous, and peraluminous regions, where only Na_2O, Al_2O_3, B_2O_3, and SiO_2 were included, with and without La_2O_3. The amount of B_2O_3 was kept constant, while the amounts of Na_2O, Al_2O_3, and SiO_2 were varied. These glasses are still under investigation and data will be presented elsewhere.

Effects of Ti, Ru, and Zr

Finally, the effects of other minor components have been considered. First, it was found that small additions of TiO_2 to MoO_3-containing borosilicates favored the water-durable phase ($CaMoO_4$) and inhibited the formation of water-soluble phase (Na_2MoO_4), possibly by requiring charge compensation of the four coordinated titanium by Na^+ in the glass, thus suppressing the formation of Na_2MoO_4 crystals. Ti-containing glasses were melted and crystallized, and studied by XRD, SEM, Raman spectroscopy and thermal analysis. Also, ^{23}Na MAS NMR analysis was performed to determine the relative percentage of sodium present in the crystalline phase (Na_2MoO_4) and amorphous phase in the glass-ceramic. Detailed results will be published elsewhere.

Sequential additions of ZrO_2 to Nd- and Mo-containing glasses were also investigated. Progressive addition of ZrO_2 appeared to produce the kinetically delayed formation of oxyapatite. ZrO_2 addition also reduced the fraction of four-coordinated boron units, again presumably due to the requirements of charge compensation of ZrO_2 by Na [16]. Additions of RuO_2 to these ZrO_2-containing glasses have also been made, and results are under investigation. The fully analyzed data will be presented elsewhere.

3. RESULTS AND DISCUSSION

Though much of the work alluded to in this summary paper are already or will soon be published elsewhere, some important characteristics of the overall study set are pointed out here. A typical microstructure for a slow-cooled glass ceramic is shown in Figure 1.

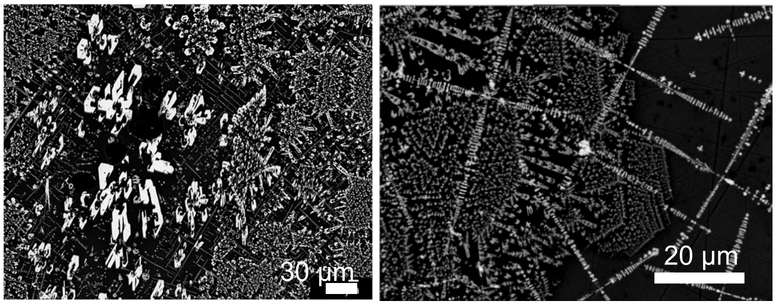

Figure 1- Backscattered SEM microstructure of a typical slow-cooled peralkaline glass-ceramic (here LaNaCaMo, left, and YNaCaMo, right). Note the presence of various morphologies of bright oxyapatite crystals, both large and small arrays, mostly of skeletal nature. Also, note two morphologies for grey powellite, large skeletal crystals, as well as small dendrite 'crosses' within the residual glass.

Kinetics

Some limited kinetic studies have been made of previously studied glasses [8], such as that shown in Figure 2. Isothermal holds starting at 700°C for high MoO_3 (RE-3Mo) and 800°C for lower MoO_3 show signs of opacity, which continue through the maximum temperature investigated (1200°C). Raman spectra (Figure 2) show the presence of powellite [9] starting at 700°C heat treatment for RE-3Mo and 800°C heat treatment for RE-2Mo. The broad band at 914-916 cm^{-1} in MoO_3-containing glasses is due to the symmetric stretch of isolated MoO_4^{2-} units (see [9] and references therein). The 1020 cm^{-1} band is due to trigonal BO_3 units in the glass, and the ~861–863 cm^{-1} band is due to oxyapatite crystals [18].

Differential thermal analysis scans were also collected on these glasses to study their crystallization behavior. Glass powders in the particle size 0.85–1.0 mm were used to perform DSC scans in the temperature range of 30–1500°C and four different heating rates (5, 10, 15 and 20 °C/min). Activation energies of crystallization of all the glasses were calculated using the Augis-Bennet equation (Equation 1).

$$\ln\left(\frac{\beta}{T_p}\right) = -\frac{E_c}{RT_p} + \ln k_0 \qquad (1)$$

where β is the heating rate, T_p is the peak of crystallization temperature, E_c is the activation energy of crystallization and k_0 is a constant. The linear fitting (with the least square method) of the experimental results to Equation 1 for the studied glasses (along with the correlation coefficients, R^2) is shown in Figure 3, along with the values of the activation energies. It was found that the activation energy of crystallization decreased with increasing MoO_3 content from 0–2 mol% and then increased with increase in the MoO_3 concentration to 3 mol%. A similar trend was observed in the liquidus temperature of these samples. The liquidus temperatures were measured on a 20 mesh glass powder in a platinum boat by ASTM–C829-810 and crystals were detected by microscopic techniques at 150× magnification. EDS analysis suggested that Ca-Nd oxyapatite was the first crystal phase that appeared at the liquidus temperature.

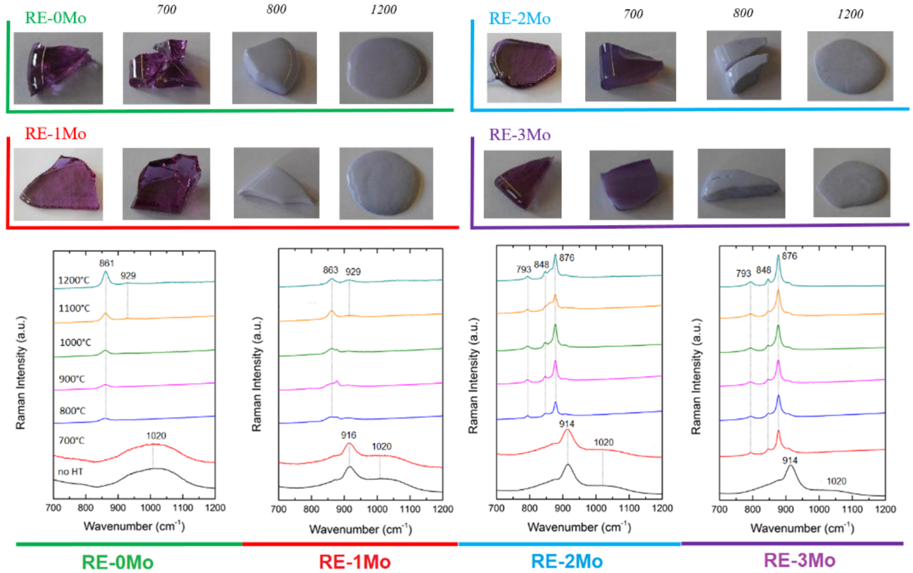

Figure 2- (Top) Photographs of RE-*x*Mo samples isothermally heat treated at different temperatures; (Bottom) Raman spectra after heat treatment; temperatures shown in leftmost figure are the same across all four figures; some peaks are labeled with their wavenumber.

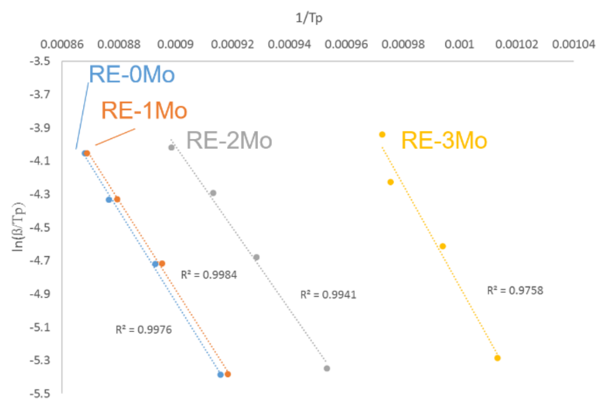

Glass	E_c (±5) (kJ/mole)	Liquidus T (±3) (°C)
RE-0Mo	228	1330
RE-1Mo	223	1325
RE-2Mo	204	1307
RE-3Mo	255	1332

Figure 3- (Left) Plots according to Augis-Bennet Equation (Equation 1) to calculate activation energy of crystallization. (Right) The activation energy of crystallization and liquidus temperature of glasses in the series RE-*x*Mo

Glass structure around RE and Mo

The effect of composition on glass structure, particularly around the RE and Mo cations, was of particular interest. Current and previous studies have used XAS measurements (including XANES and EXAFS) to study the Mo [9, 11, 19-21] and RE [16, 22, 23] environments. Raman spectroscopy has also been used to investigate glass structure, particularly given the strong vibrational signature of MoO_4^{2-} units [9, 14, 18, 21, 24].

Some studies have also looked at NMR [8, 23, 25-31] of ^{29}Si, ^{27}Al, ^{23}Na, ^{11}B, and ^{17}O, and in rare cases ^{139}La, ^{95}Mo, or ^{133}Cs. However, glasses containing a substantial fraction of paramagnetic RE oxides are problematic for NMR experiments. Figure 4 shows the magnetic susceptibility of the RE cations as derived from [32, 33] along with ionic (crystal) radii of the trivalent RE [34]. Note that Y and Sc, though not shown on the RE ion plot, are non-paramagnetic, but are included in size sequence in Figure 4.

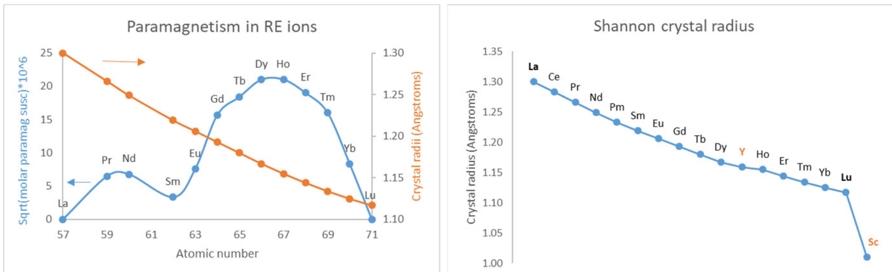

Figure 4- Relative paramagnetism and ionic size of trivalent lanthanide RE plus Y and Sc.

Figure 5 shows ^{11}B MAS NMR spectra of glasses containing 4.93 mol% (total) of single and mixed oxides of Nd, Er, Sm, La, Lu, Sc, and Y. For the glasses containing paramagnetic ions, the effect is strongest for Er, the most paramagnetic, and it destroys the spectrum when present at the full amount; however, some structure is still visible when it is present only in 0.93 mol% Er_2O_3 (+4 mol% La_2O_3). The Yb sample is also mostly damped out, while the Sm sample has some shifting in addition to the damping. The Nd-La series shows a progressive broadening and possibly some selective damping of one of the B components. For the comparison of the non-paramagnetic ions (La, Lu, Y, Sc), there is evidence of a trend toward higher fractions of BO_3 units with smaller RE cations. There is also some indication that RE ions may partition close to certain types of boron units, such as ring or non-ring [35].

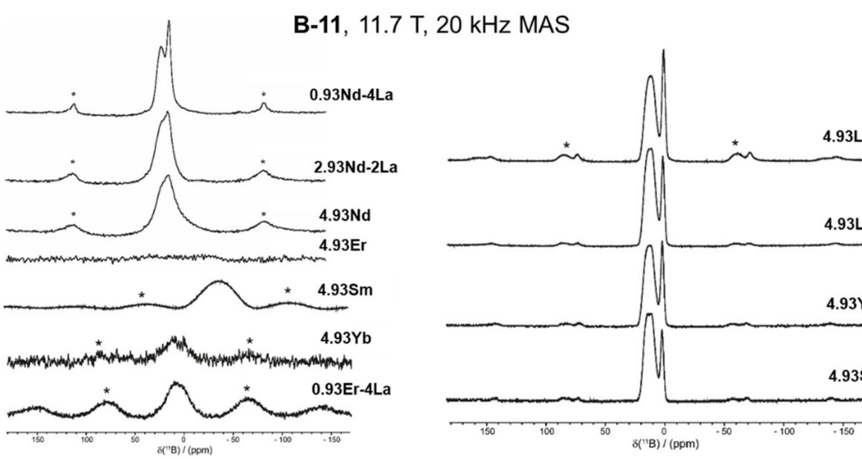

Figure 5- ^{11}B NMR spectra of RE oxide containing glasses (RENaCaMo (indicated as 4.93RE, La-Nd, La-Er series in Table 1). Note that the total RE oxide concentration in all samples shown is 4.93 mol%. Stars indicate spinning sidebands.

Another characterization method that is sometimes used for studying the structure around RE is visible absorption. Given the abundance of electronic transitions in the visible frequency range for trivalent lanthanide RE ions [36], absorption measurements and/or luminescence measurements can give useful information about RE local environment in glasses. This technique has been used a great deal for nuclear waste glasses, particularly the transitions of Nd^{3+} [7, 14, 15, 18, 23, 37-39], though occasionally other RE^{3+} are used [40]. Figure 6 shows the absorbance of polished plates of selected quenched glasses, as well as an example of combined excitation emission spectroscopy (CEES) for Er^{3+} in the glass. Other than the focus on Nd^{3+}, these absorption-emission techniques seem underutilized in the literature.

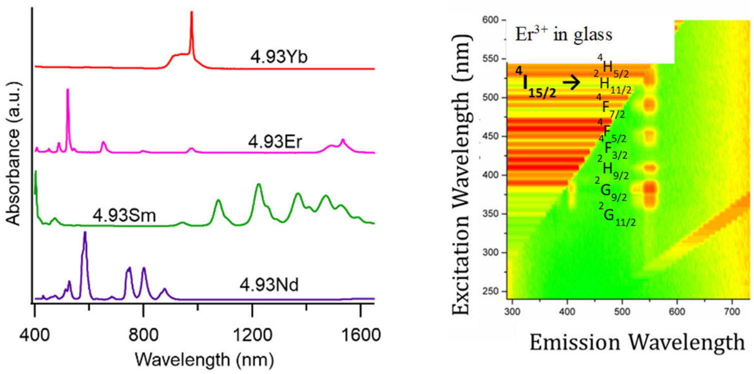

Figure 6- (Left) Optical absorbance of RE oxide containing glasses (RENaCaMo series in Table 1, offset for clarity). (Right) Combined Excitation and Emission Spectroscopy (CEES), also known as PL/PLE, of 4.93Er (also known as ErNaCoMo glass); some specific electronic absorption (excitation) transitions observed in the spectrum are labeled.

Partitioning of rare earths into various crystal phases

Non-paramagnetic RE analogues with different sizes (La, Y, Lu, Sc) were prepared to allow NMR study, as discussed previously. These glasses were also heat treated to assess crystals formed. As before, all formed powellite (~5 mass%). The La glass formed oxyapatite [9], as did the Y glass, though EPMA and XRD suggested that the stoichiometry of the Y-apatite is closer to $Ca_4Y_6Si_5O_{25}$ (i.e., Ca-rich and O-poor). The Lu glass formed 1.5 mass% of a keiviite-structured $Lu_2Si_2O_7$, whose existence had been reported previously [41, 42]. Surprisingly, the Sc glass did not form $Sc_2Si_2O_7$ (thortveitite), but rather only powellite. This is possibly because the natural mineral thortveitite normally contains substantial Y, which is a much larger cation [43].

Throughout these studies, it has been found that the RE in these systems can be associated with many different phases. For peralkaline glasses, the main RE phase was oxyapatite, but small RE cations (Tm, Yb, Lu) favor a keiviite or related phase. Peraluminous behavior was more complicated, in that crystallization of silicate phases (oxyapatite, $RE_2Si_2O_7$), borate phases ($REBO_3$), and borosilicate phases ($RE_3BSi_2O_{10}$) were observed depending on the RE involved. These results lend support for suggestions given by Qian et al. [44] for Gd present in borate, silicate, or borosilicate environments depending on glass composition. In addition to these phases, RE was always found in some amount in powellite. When a Zr-related phase crystallized [i.e., cerianite $(Ce, Zr)O_2$ in Ce-containing peralkaline glasses or various ZrO_2-related phases in peraluminous glasses], the phase invariably contained some RE, which often stabilized a tetragonal or even cubic ZrO_2 phase.

It should be recognized that many of the observed phases appear quite flexible regarding accommodation of some amount of Ca, Zr, and/or RE^{3+} in their structure. For example, keiviite phases contain some Ca and Zr in addition to RE. Oxyapatite phases contain Ca and RE to various degrees, and probably also some Zr, B, and Na [9]. Lanthanide borosilicate crystalline phases appear to be mostly RE, B, and Si, however. Powellite contains mostly Ca and Mo, but some Na and RE as well. As previously stated, the ZrO_2 phases usually contain some RE. A complete description of these phenomena is planned for a future publication.

4. CONCLUSIONS

A comprehensive study has been undertaken in a partnership between US and UK researchers to study the glass and glass-ceramic systems for nuclear waste management in the alumino-boro-silicate system containing various metals (alkali, alkaline earth, rare earth, transition metal). Several series of simplified glasses were fabricated and crystallized, then studied using a suite of techniques. Overall, several findings can be summarized. It was found that the solubility of Mo can be increased in glass by adding RE or Ti. Peralkaline glasses generally formed oxyapatite and powellite phases. Glasses with only small RE cations formed a different silicate crystal based on keiviite. Peraluminous glasses formed more complex suites of crystalline phases, depending strongly on the RE cation size. More work is needed to fully understand these preliminary results. It is likely that both RE cation size and Na distribution for charge compensation of various moieties (AlO_4^-, ZrO_6^{2-}, BO_4^-, MoO_4^{2-}, and RE-O species) plays a significant role on the specific crystallization behavior. Readers are advised to refer to future detailed publications expanding upon this preliminary report.

ACKNOWLEDGMENTS

The authors gratefully acknowledge research funding from the U.S. Department of Energy (US DOE) Office of Nuclear Energy and the Nuclear Engineering University Program (NEUP), contract # DE-NE0008431. This work was, in part, performed in the MIDAS facility at the University of Sheffield, for which the financial support of the Department of Energy and Climate Change is gratefully acknowledged. The UK portion of the research was sponsored, in part, by the UK Engineering and Physical Sciences Research Council under grant references EP/N017870/1, EP/N017617/1, and EP/P013600/1. JVH thanks the EPSRC, the University of Warwick and the Birmingham Science City Program for partial funding of the solid-state NMR infrastructure at Warwick. The latter program accessed the Birmingham Science City Advanced Materials Project 1: Creating and Characterising Next Generation Advanced Materials, which derived support from Advantage West Midlands (AWM) and the European Regional Development Fund (ERDF). Pacific Northwest National Laboratory is operated by Battelle Memorial Institute for the US DOE under contract DE-AC05-76RL01830.

REFERENCES

1 J.V. Crum, L. Turo, B. Riley, M. Tang and A. Kossoy, J. Am. Ceram. Soc. **95**, 1297 (2012).

2 J. Crum, V. Maio, J. McCloy, C. Scott, B. Riley, B. Benefiel, J. Vienna, K. Archibald, C. Rodriguez, V. Rutledge, Z. Zhu, J. Ryan and M. Olszta, J. Nucl. Mater. **444**, 481 (2014).

3 J.D. Vienna, J.V. Crum, G.J. Sevigny and G.L. Smith, Preliminary Technology Maturation Plan for Immobilization of High-Level Waste in Glass-Ceramics, Pacific

Northwest National Laboratory, Richland, WA, PNNL-21714, FCRD-SWF-2012-000152 (2012).
4 S. Tan, M.I. Ojovan, N.C. Hyatt and R.J. Hand, J. Nucl. Mater. **458**, 335 (2015).
5 Assessment of the State of the Art of HLW and ILW Processing Technologies for Fast Reactor Recycle Wastes, National Nuclear Laboratory NNL(13)12536 (2013).
6 The UK's Nuclear Future, Department for Business, Innovation and SkillsHM Government Industrial Strategy Report (2013).
7 J.S. McCloy, B. Riley, J. Crum, J. Marcial, J. Reiser, K. Kruska, J. Peterson, D. Neuville, D. Patil, K. Barnsley and J.V. Hanna, (submitted).
8 A. Brehault, D. Patil, H. Kamat, R.E. Youngman, L.M. Thirion, J.C. Mauro, C.L. Corkhill, J.S. McCloy and A. Goel, J. Phys. Chem. B **122**, 1714 (2018).
9 D.S. Patil, M. Konale, M. Gabel, O.K. Neill, J.V. Crum, A. Goel, M.C. Stennett, N.C. Hyatt and J.S. McCloy, J. Nucl. Mater. **510**, 539 (2018).
10 J. McCloy, J. Marcial, B. Riley, J. Neufeind, J. Crum and D. Patil, MRS Adv. (accepted).
11 G. Calas, M. Le Grand, L. Galoisy and D. Ghaleb, J. Nucl. Mater. **322**, 15 (2003).
12 C. Martineau, V.K. Michaelis, S. Schuller and S. Kroeker, Chem. Mater. **22**, 4896 (2010).
13 N. Chouard, D. Caurant, O. Majérus, J.L. Dussossoy, S. Klimin, D. Pytalev, R. Baddour-Hadjean and J.P. Pereira-Ramos, J. Mater. Sci. 1 (2014).
14 N. Chouard, D. Caurant, O. Majérus, J.L. Dussossoy, A. Ledieu, S. Peuget, R. Baddour-Hadjean and J.P. Pereira-Ramos, J. Non-Cryst. Solids **357**, 2752 (2011).
15 O. Majérus, D. Caurant, A. Quintas, J.-L. Dussossoy, I. Bardez and P. Loiseau, J. Non-Cryst. Solids **357**, 2744 (2011).
16 A. Quintas, D. Caurant, O. Majérus, P. Loiseau, T. Charpentier and J.-L. Dussossoy, J. Alloys Compd. **714**, 47 (2017).
17 D. Perret, I. Bardez-Giboire, J.L. Dussosoy, N. Bousquet and F. Baudet in *JMP Discovery Summit,* 2011, https://community.jmp.com/kvoqx44227/attachments/kvoqx44227/discovery, accessed 1 Dec 2018.
18 N. Chouard, D. Caurant, O. Majérus, N. Guezi-Hasni, J.-L. Dussossoy, R. Baddour-Hadjean and J.-P. Pereira-Ramos, J. Alloys Compd. **671**, 84 (2016).
19 F. Farges, R. Siewert, G.E. Brown, A. Guesdon and G. Morin, Canad. Mineral. **44**, 731 (2006).
20 N.C. Hyatt, R.J. Short, R.J. Hand, W.E. Lee, F. Livens, J.M. Charnock and R.L. Bilsborrow, In *Environmental Issues and Waste Management Technologies in the Ceramic and Nuclear Industries X*, edited, (John Wiley & Sons, Inc., 2006), pp. 179.
21 D.A. McKeown, H. Gan and I.L. Pegg, J. Nucl. Mater. **488**, 143 (2017).
22 C.W. Ponader and G.E. Brown, Geochim. Cosmochim. Acta **53**, 2893 (1989).
23 H. Trégouët, D. Caurant, O. Majérus, T. Charpentier, L. Cormier and D. Pytalev, Procedia Mater. Sci. **7**, 131 (2014).
24 I. Bardez, D. Caurant, P. Loiseau, N. Baffier, J.L. Dussossoy, C. Gervais, F. Ribot and D.R. Neuville, Phys. Chem. Glasses **46**, 320 (2005).
25 A. Quintas, D. Caurant, O. Majérus, T. Charpentier and J.L. Dussossoy, Mat. Res. Bull. **44**, 1895 (2009).
26 E. Nicoleau, F. Angeli, S. Schuller, T. Charpentier, P. Jollivet and M. Moskura, J. Non-Cryst. Solids **438**, 37 (2016).
27 S. Kroeker, S. Schuller, J.E.C. Wren, B.J. Greer and A. Mesbah, J. Am. Ceram. Soc. **99**, 1557 (2016).
28 M. Magnin, S. Schuller, C. Mercier, J. Trébosc, D. Caurant, O. Majérus, F. Angéli and T. Charpentier, J. Am. Ceram. Soc. **94**, 4274 (2011).
29 D. Caurant, O. Majérus, E. Fadel, A. Quintas, C. Gervais, T. Charpentier and D. Neuville, J. Nucl. Mater. **396**, 94 (2010).
30 S. Kroeker, C.S. Higman, V.K. Michaelis, N.B. Svenda and S. Schuller, Mater. Res. Soc. Symp. Proc. **1265**, (2010).
31 F. Angeli, O. Villain, S. Schuller, S. Ispas and T. Charpentier, Geochim. Cosmochim. Acta **75**, 2453 (2011).
32 K.P. Belov, A.M. Kadmtseva and R.Z. Levitin, Sov. Phys. JETP **20**, 291 (1965).
33 X. Bohigas, J. Lluma, J. Tejada, L.L. Vistin, N.I. Sorokin and B.P. Sobolev, Bull. Soc. Cat. Cien. **13**, 273 (1992).
34 R.D. Shannon, Acta Crystallog. A **32**, 751 (1976).
35 E. Nicoleau, S. Schuller, F. Angeli, T. Charpentier, P. Jollivet, A. Le Gac, M. Fournier, A. Mesbah and F. Vasconcelos, J. Non-Cryst. Solids **427**, 120 (2015).
36 M.J. Dejneka, A. Streltsov, S. Pal, A.G. Frutos, C.L. Powell, K. Yost, P.K. Yuen, U. Müller and J. Lahiri, Proc. Natl. Acad. Sci. U. S. A. **100**, 389 (2003).
37 D. Caurant, Opt. Spectrosc. **116**, 667 (2014).
38 I. Bardez, D. Caurant, J.L. Dussosoy, P. Loiseau, C. Gervais, F. Ribot, D. Neuville, N. Baffier and C. Fillet, Nucl. Sci. Eng. **153**, 272 (2006).
39 A. Kidari, J.-L. Dussossoy, E. Brackx, D. Caurant, M. Magnin and I. Bardez-Giboire, J. Am. Ceram. Soc. **95**, 2537 (2012).
40 A. Winterstein-Beckmann, D. Möncke, D. Palles, E.I. Kamitsos and L. Wondraczek, J. Phys. Chem. B **119**, 3259 (2015).

41 H. Ohashi, M.D. Alba, A.I. Becerro, P. Chain and A. Escudero, J. Phys. Chem. Solids **68**, 464 (2007).
42 F. Soetebier and W. Urland, Z. Kristallogr. - New Cryst. Struct. **217**, 22 (2002).
43 E.E. Foord, S.D. Birmingham, F. Demartin, T. Pilati, C.M. Gramaccioli and F.E. Lichte, Canad. Mineral. **31**, 337 (1993).
44 M. Qian, L. Li, H. Li and D.M. Strachan, J. Non-Cryst. Solids **333**, 1 (2004).